DVMark: A Deep Multiscale Framework for Video Watermarking

Xiyang Luo[1], Yinxiao Li[1], Huiwen Chang[1], Ce Liu[1], Peyman Milanfar[1], and Feng Yang[1]
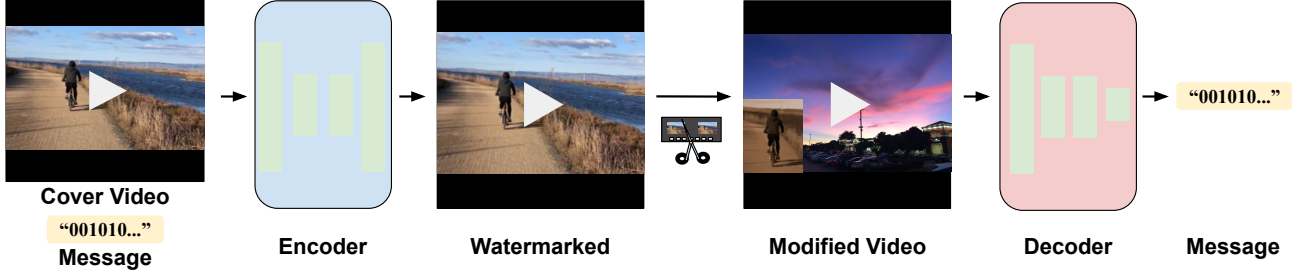
[1]Google Research

Figure 1: DVMark hides a message into a video which can be robustly recovered. The encoder network takes a cover video and a binary message, and generates a watermarked video that appears identical to the human eye as the input. The watermarked message can still be reliably extracted by our decoder even if the video undergoes a series of common video editing operations, such as compression, crop, color shift, and padding the watermarked video with other video content.

Abstract

Video watermarking embeds a message into a cover video in an imperceptible manner, which can be retrieved even if the video undergoes certain modifications or distortions. Traditional watermarking methods are often manually designed for particular types of distortions and thus cannot simultaneously handle a broad spectrum of distortions. To this end, we propose a robust deep learning-based solution for video watermarking that is end-to-end trainable. Our model consists of a novel multiscale design where the watermarks are distributed across multiple spatial-temporal scales. It gains robustness against various distortions through a differentiable distortion layer, whereas non-differentiable distortions, such as popular video compression standards, are modeled by a differentiable proxy. Extensive evaluations on a wide variety of distortions show that our method outperforms traditional video watermarking methods as well as deep image watermarking models by a large margin. We further demonstrate the practicality of our method on a realistic video-editing application.

1. Introduction

Watermarking is the problem of embedding messages in a cover media, such as images, video, or audio. Watermarks can be either visible or invisible. Invisible watermarks come with the benefit of being non-obtrusive to the original con-

tent, as well as making it more difficult to identify and detect for a potential attacker. In this paper we focus on the problem of invisible watermarks for videos, and refer to it as video watermarking throughout the rest of the paper.

There are three major factors to consider when evaluating a video watermarking system, namely, imperceptibility (or quality), robustness to various distortions, and number of message bits (payload or capacity). These factors are in tension with each other. For example, increasing robustness often comes at a price of lowering visual quality, and increasing the payload may have a non-trivial impact on both decoding accuracy as well as visual quality. The trade-offs between these factors determine the overall performance of a watermarking system.

Traditional watermarking methods rely on hand-designed features to improve the system along these factors, such as applying various transforms or using perceptual masking [4, 7]. There are several drawbacks to a hand-crafted approach. First of all, different types of distortions often require different techniques, and therefore most traditional methods are not simultaneously robust to all types of distortions [5]. Secondly, a hand-designed system often lacks the power to fully exploit the rich spatial-temporal information in a given video, leading to sub-optimal performance. Recently deep learning based methods have been developed for image watermarking with promising results [50, 42, 31]. However, directly applying these deep image watermarking models to videos does not fully ex-
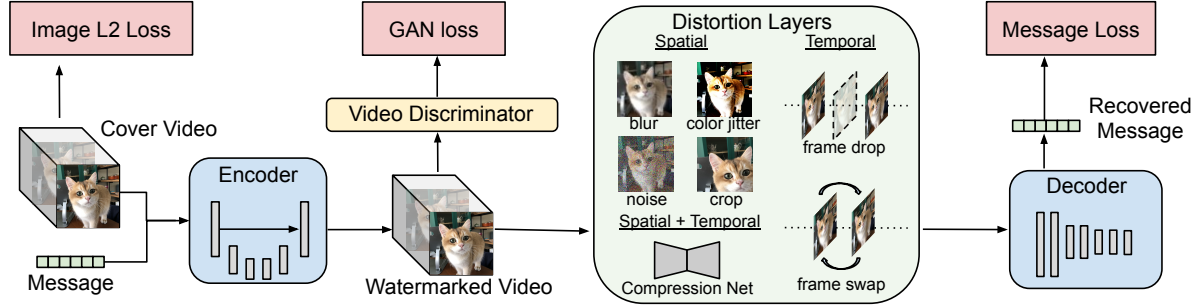
Figure 2: Our model consists of four main components, an encoder, a distortion layer, a decoder, and a video discriminator. The encoder takes as input a cover video and a binary message, and produces a watermarked video. The distortion layer applies a variety of distortions such as frame dropping, cropping, and compression to the watermarked video. The decoder network produces a predicted message from the distorted video. The video discriminator is trained to differentiate between the watermarked and cover videos, for the purpose of improving perceptual quality and temporal consistency.

plore the temporal correlations in a video, resulting in a sub-optimal robustness-quality-payload trade-off (see Figure 7, and Figure 8).

There are many challenges to designing a deep video watermarking method. For example, video compression is not differentiable and hard to incorporate in an end-to-end training framework. Moreover, it is non-trivial to design a robust model that fully utilizes the temporal correlations in a video while retaining good temporal consistency and perceptual quality. In this paper, we propose a highly robust deep video watermarking method that addresses all these issues. Below is a summary of our main contributions.

- We propose DVMark, a highly robust deep learning based solution for video watermarking. Through rigorous evaluations on robustness, quality, capacity, as well as video distortions, we demonstrate that our method outperforms previous baselines by a significant margin. We further prove the practicality of our method by testing on multiple video resolutions and lengths, as well as on a video-editing application.

- Our proposed method incorporates a novel multiscale design in both the encoder and decoder, where the messages are embedded across multiple spatial-temporal scales. This design brings more robustness compared to a single-scale network.

- We propose an effective solution for improving robustness towards video compression through the use of a differentiable proxy.

- Due to the prevalence of video editing, many videos may contain a mixture of watermarked and unwatermarked content. Therefore, we propose augmenting the decoder network with a watermark detector for detecting which frames are watermarked. This novel design gives the ability to precisely locate the watermarked frames.

2. Related Work

Watermarking digital media [15, 23, 6, 21, 35, 39, 41, 19] is an important and active area of research. Traditional video watermarking can be roughly classified into three groups: spatial domain, compressed domain, and transform domain methods, based on the domain it acts on [5].

Spatial domain methods embed the watermark by directly modifying the pixel values of the cover video. One example is Least Significant Bits (LSB) [22, 11], which is lacking in terms of robustness. More advanced spatial domain methods such as block-based methods [26] or feature-point methods [25] addresses some of the weaknesses of LSB. Compression domain methods are designed to work for a specific video codec, such as the popular H.264 [47]. Zhang *et al.* [48] proposed a method compatible with the H.264, where the watermark is embedded in the DCT coefficients. One drawback of this approach is that the watermark is format specific, and does not support conversion using an alternative codec.

The third group of methods apply certain transforms to the cover video prior to embedding the watermark message. Popular transforms include Discrete Fourier Transform (DFT) [16], and Discrete Cosine Transform (DCT) [17], *etc*. More complex transforms, such as the Discrete Wavelet Transform (DWT) [32, 10, 28, 7] and the Dual-tree Complex Wavelet Transform (DT-CWT) [13, 4, 1], have also yielded good performance in terms of robustness and quality. In addition, techniques such as perceptual masking based on the Human Visual System (HSV) [40, 7] further improve the perceptual quality for many traditional watermarking methods. A comprehensive survey for video watermarking could be found in [5, 36].

Deep learning based approaches have recently been gaining traction in the field of watermarking, due to its impressive performance in terms of robustness and perceptual quality [50, 2, 46, 42, 45]. HiDDeN [50] was one

of the first deep learning solutions for image watermarking. RedMark [2] proposed extensions to the HiDDeN framework through the use of space-to-depth transforms and circular convolutions. Several works also focus on dealing with modelling more complex and realistic distortions [42, 46, 31]. StegaStamp [42] models the camera capture distortion via a sequence of primitive transforms such as color-change, blurring, and perspective warping. Wengrowski *et al.* [46] proposed training a deep neural network to simulate screen display distortions. Liu *et al.* [29] proposed a two stage pipeline for training robust models against style transfer distortions. Applying image watermarking methods to videos results in a sub-optimal performance in terms of robustness and quality, since these methods are not able to utilize any temporal correlations between video frames.

For videos, VStegNet [33] from Mishra *et al.* achieved great performance for the task of video steganography. We note the difference with our work since VStegNet does not consider video distortions. The presence of even minor distortion greatly affects the quality and robustness of a model, and it is a non-trivial task to maintain both high perceptual quality and robustness.

Generative Adversarial Network (GAN)-based training [18] is another important technique for deep learning based image and video processing for improving the perceptual quality of the generated videos. Techniques such as Wasserstein GANs [3] and spectral normalization [34] have greatly stabilized the training process. Some notable applications image and video processing where GANs were used include ESRGAN [44], TecoGAN [12], MOCOGAN [43].

3. Proposed Method

We propose an end-to-end trainable model for embedding a binary message of length m to n video frames. As shown in Figure 2, our framework consists of four modules, an *encoder*, a *decoder*, a *distortion layer*, and a *video discriminator*. We explain in more detail each of the components below.

3.1. Encoder

The encoder network takes a cover video and an input message as input, and outputs the watermarked video. Figure 3 (top) shows the architecture of the encoder network. The encoder consists of two main components: the *transform layer* and the *embedding layer*. The transform layer maps the input video sequence to a feature map of the same dimensions as the input. The embedding layer then outputs a watermark residual R. This is added to the original video multiplied by a scalar factor α, *i.e.*,

$$V_w = V_{in} + R \times \alpha, \tag{1}$$

where V_{in} is the cover video, V_w the watermarked video, α an adjustable watermark strength factor used to control the trade-off between quality and robustness.

Transform Layer: The transform layer consists of 4 layers of 3D convolutions which transform the input video block to a 3D feature block with the same spatial-temporal dimensions. Each layer has 64 output channels, with stride equal to 1, spatial kernel size equal to 3, and temporal kernel size equal to 1, 1, 1, 3 respectively. This design is inspired by traditional watermarking methods in the frequency-domain where the messages are embedded onto a transformed video instead of directly on the pixel domain. The transform layer thus allows us to learn an optimal transformation prior to merging with the messages.

Embedding Layer: The embedding layer (Figure 3) fuses the input message M with the transformed video features at two scale levels S_1 and S_2. To merge the message with the video features, we first repeat the message along the spatial-temporal dimensions and concatenate with the feature map along the channel dimension. If the video feature map is a tensor of shape $t \times h \times w \times c$, the repeated message block has shape $t \times h \times w \times m$, with m being the message length. For the first scale level S_1, We apply three Conv3D operations with kernel size 3 and number of channels 256, 128, 128 to the concatenated feature map. This operation is indicated by the yellow arrow labelled "Multiple Conv3D" in Figure 3. For the second scale level S_2, we apply a AvgPool3D to perform a 2X downsampling of the feature map from S_1 to S_2. We repeat the same process of concatenating with the message and applying Conv3D operations with channels 512, 256, 256 before upsampling through bilinear interpolation S_1.

3.2. Decoder

The decoder network takes a possibly distorted version of the watermarked video V_d, and outputs a decoded message M^w. Similar to the encoder, our decoder also incorporates a multi-scale component through a multi-head design. We further predict a per-video weight vector for each decoder head, so that the distribution strategy across different scales can be content-adaptive. The weights are learned through a small network named WeightNet. Finally, we propose augmenting an additional head for the purpose of detecting whether a video has been watermarked. This has important practical implications since detecting whether a video (or parts of a video) has been watermarked is often as an important task as extracting the message itself.

Transform Layer: We first apply a transformation layer to map the distorted video V_d to a feature map D_f which will be shared by both the decoder and detector heads. We apply four Conv3D operations same as in the encoder transformation layer to extract the feature maps. In traditional frequency-based methods, the decoder usu-
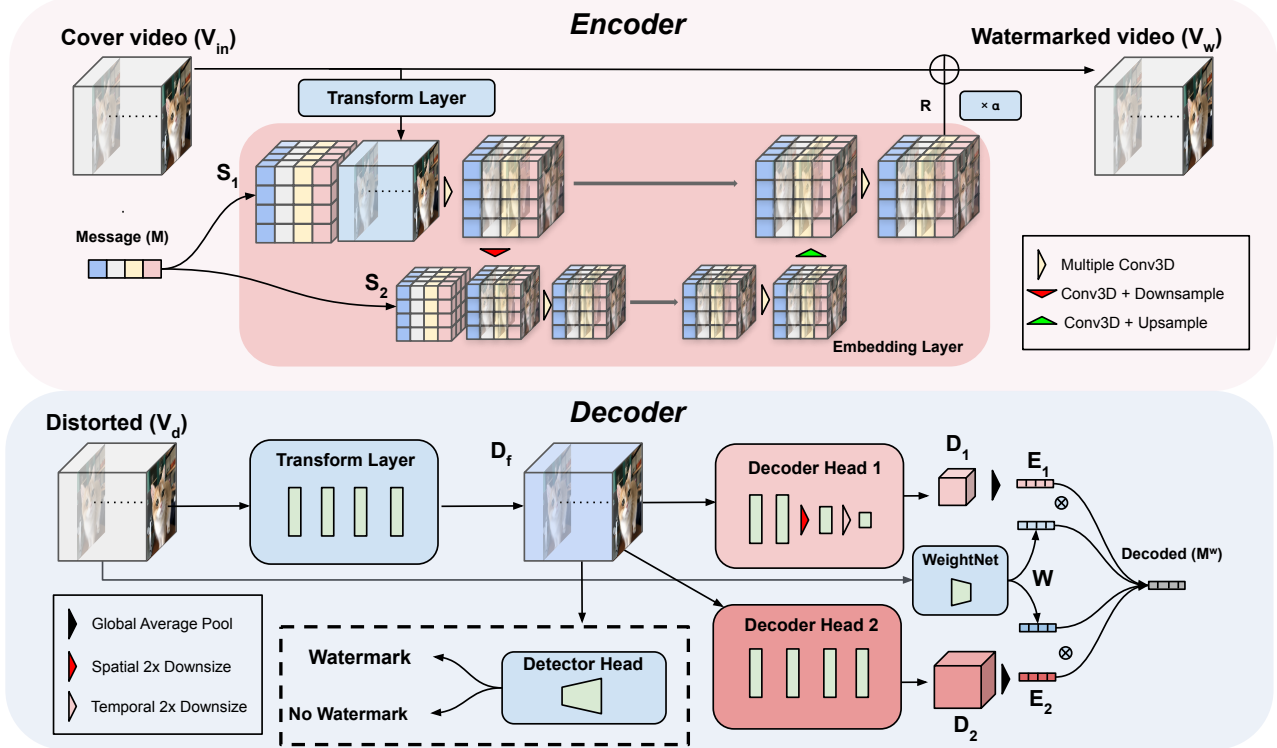
Figure 3: Architecture of the multiscale encoder and decoder networks for DVMark. The encoder network fuses the input message with the cover video through a multiscale network on two different spatial-temporal scales. The input message is first repeated across spatial and temporal dimensions, and then fused with activations of the transformed cover video. The encoder learns a residual mapping which is added back to the cover video to obtain the watermarked video. A scalar factor could be multiplied to the residual to adjust the watermark strength at inference time. The decoder network consists of a transform layer and two detector heads which generates a decoded message map of different scales. The decoded maps are globally average pooled and linearly merged by a weight matrix of the same length predicted from a small network. The decoder is further augmented with a detector head with the ability to distinguish watermarked frames from unwatermarked frames.

ally applies the same frequency transforms as the encoder, but we allow the flexibility of learning different transformations for the decoder in our design.

Multi-head Decoder: In our multi-head design, each decoder head outputs a decoded block D_i with the same dimensions as each scale level S_i. For example with a training video size of $8 \times 128 \times 128 \times 3$, $D_1 \in \mathbb{R}^{4 \times 64 \times 64 \times m}$ and $D_2 \in \mathbb{R}^{8 \times 128 \times 128 \times m}$. Each decoder head contains four Conv3D$_{3,3,3}$ operations, where the output channels are 128,128,256,512 for head 1, and 128,128,128,256 for head 2. A 2X average pooling is applied to the spatial and temporal dimensions for the last two layers in head1. We then apply global average pooling to the blocks D_i to obtain a decoded vector $E_i \in \mathbb{R}^m$, which represents the decoded information from each decoder head. Namely,

$$M^w = W^T E. \qquad (2)$$

The weight matrix W_{ij} represents the importance of the predictions from scale i for each bit j. W is predicted per-video from a small network named WeightNet.

Watermark Detector: The watermark detector predicts whether a frame has been watermarked by the DVMark encoder or not. We observed that the feature maps learned from the transform layer can be re-used to differentiate between watermarked and unwatermarked video frames. Therefore, we train a detector head to differentiate watermarked frames from unwatermarked frames under the presence of various distortions. The detector head consists of four Conv2D$_{3,3}$ operations, where the output channels are 128,128,256,512 respectively.

3.3. Distortion Layer

Robustness to a broad variety of distortions has always been a challenge for traditional video watermarking methods. In our framework, we achieve this by using a combination of common distortions during the training process. The distortions consist of temporal distortions, spatial distortions, as well as a differentiable version of video compression. At training time, each distortion is selected randomly with equal probability for each step of training. By randomly injecting distortions during the training process, both the encoder and decoder learn to be simultaneously ro-

bust to a variety of different distortions.

CompressionNet: Robustness to video compression is a crucial requirement for a video watermarking method. Traditional video watermarking methods improve their robustness by embedding messages in the mid-low frequency components in a video. However, manipulations on the frequency domain alone cannot not fully capture the complexity of video codecs. To more accurately simulate video compression, we train a small 3D-CNN, named CompressionNet, to mimic the output of an H.264 codec at a fixed Constant Rate Factor (CRF) [47]. With CRF = 25, the final trained network gives a PSNR of 33.3dB with respect to the real compressed output. We then fix the weights of CompressionNet and apply it as a distortion when training the video watermarking model.

3.4. Video Discriminator

Temporal consistency is an important issue for any video processing or generation tasks. Inspired by recent advances in video generations [37, 43], we tackle this issue by employing a multiscale video discriminator from TGAN2 [37]. As shown in Figure 4, the discriminator network consists of four 3D residual networks, each taking a different temporal and spatial resolution of the input video.
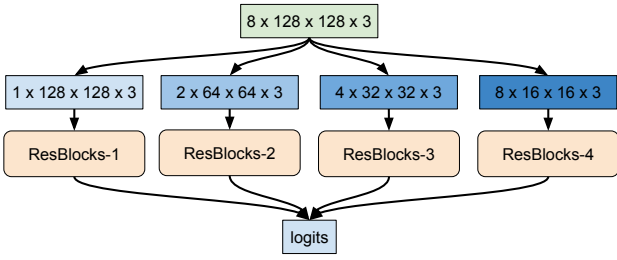

Figure 4: Architecture of the multiscale video discriminator. Each 3D ResBlock processes an input of varying resolutions, allowing the network to capture both spatial and temporal differences between the cover and watermarked videos.

Given the discriminator D, the generator and discriminator losses are given by the Hinge loss formulation [30]. The discriminator optimizes L_D while L_G (see Eq. 4) is added to the encoder-decoder loss in Eq. 6.

$$L_D = \max\{0, 1 - D(V_w)\} + \max\{0, 1 + D(V_{in})\} \quad (3)$$
$$L_G = -D(V_w). \quad (4)$$

We empirically observe that a powerful video discriminator is crucial for achieving good temporal consistency for our video watermarking framework. GANs trained with only 2D convolutions in image space tend to exhibit more flickering compared to our models with 3D convolutions.

3.5. Training

Encoder and Decoder: We first define the loss function which the encoder and decoder jointly optimize. Let V_{in},

V_w denote the input and output of the encoder network, M and M^w denote the input and predicted message, we define the following objective function.

$$L_{total} = L_I(V_{in}, V_w) + c_1 L_M(M, M^w) + c_2 L_G(V_w) \quad (5)$$

where c_i are the scalar weights for each loss term. Here L_I is the pixel-wise l_2-loss. L_M is the message loss given by the sigmoid cross-entropy. L_G is the Wasserstein Hinge loss from the video discriminator, where we apply spectral normalization [34] to the discriminator network. The encoder and decoder are trained jointly with respect to the loss above.

Watermark Detector: The detector is trained on top of a pre-trained encoder and decoder. For training, we randomly apply the DVMark encoder on each video clip with probability 0.5, and train the detector to predict whether the clip has been watermarked using a sigmoid cross entropy loss. Note that the weights of DVMark encoder and decoder are fixed during this process.

4. Experiments

We train and evaluate our model on the Kinetics 600 dataset [8, 9]. This dataset is a large-scale video dataset which contains about 500K 10-second clips annotated with one of 600 human action categories [24]. About 390K clips are used for training, and the rest for evaluation. We train our model on randomly cropped video clips with dimension $8 \times 128 \times 128$, and evaluate our model on 500 randomly selected videos in the Kinetics 600 validation set. We would like to emphasize that even though our model is trained on clips of size $8 \times 128 \times 128$, our model is applicable to videos of arbitrary dimensions and lengths, as indicated in Table 3.

4.1. Comparison Methods

We compare our model with both traditional transform-domain video watermarking methods, and a state-of-the-art deep image watermarking methods applied to videos.

3D-DWT Method: For the traditional method we choose a transform-domain method using 3D Discrete Wavelet Tranform (3D-DWT), a widely used technique for video watermarking method. We follow the implementation in [32], where a binary message is first transformed via the spread-spectrum technique [14] and then added to the LLH, LHL, LHH, HLL, HLH, HHL sub-bands of a 3-level DWT. We refer to this method as 3D-DWT in the rest of the paper.

HiDDeN [50]: We also compare our method with HiDDeN, a state-of-the-art deep image watermarking model robust to many image distortions, such as JPEG compression, crop and blur. For a fair comparison, we train HiDDeN with the same payload as DVMark, and apply the trained model with the same message to each video frame.

| Original | HiDDeN | 3D-DWT | DVMark |

Figure 5: Visual samples of original and watermarked video frames from various watermarking methods. From left to right: Original, HiDDeN, 3D-DWT, and DVMark. Top row contains the frames in full-view. Second row contains two zoomed-in patches for each image. The bottom row plots the normalized difference of the watermarked image with the original image, which provides a visualization of the watermarks from various methods. Please enlarge and view the images on a computer screen. We see on the zoomed-in patches (second row) that DVMark induces less visible artifacts compared to the other methods.

4.2. Method Evaluation

In this section, we compare both the robustness and visual quality of our method against the two baseline methods. To evaluate the robustness, we measure the bit accuracy, given by the percentage of bits correctly decoded. We report the bit accuracy of each model on a large collection of common distortions, including H.264, random frame drop, and frame averaging. All results in this section are evaluated on videos of size $128 \times 128 \times 8$, with payload $m = 96$.

As shown in Table 1, our method outperforms both the 3D-DWT method as well as HiDDeN by a large margin on almost all tested distortions. We also note that while the 3D-DWT method is fairly robust to some distortions such as blur and Gaussian noise, it is not robust to other types of distortions such as frame drop or crop. This echos with the remark in [5] that it is difficult for existing methods to be robust to a very broad spectrum of distortions. In contrast, our model is simultaneously robust to nearly all of the distortions in Table 1, making it a competitive method for practical applications. Figure 6 shows the decoding accuracy when the distortion level is varied. We observe that the gain is consistent across a wide range of strengths. We note that since HiDDeN is applied independently per-frame, it is naturally resistant to frame dropping. However, DVMark managed to match this performance up to a 50% drop rate.

Next, we evaluate the quality of the watermarked video with respect to the original in terms of several commonly used full-reference quality metrics, such as Peak signal-to-noise ratio (PSNR) [20], Mean Structural Similarity

(MSSIM) [20] and LPIPS [49]. We also report the tLP metric [12], which is used to specifically measure the temporal consistency of the watermarked videos. In addition to video quality metrics, we also conducted a user study to evaluate the perceptual quality of the watermarked videos. We play a 3-second clip of the encoded video and the watermarked video side-by-side, and ask raters to choose if the pair is "same", or "different". A total of 100 pairs were rated for each watermarking method, where every pair was independently rated by 5 raters. We compute the Mean-Opinion-Score (MOS) as a measure of perceptual quality. From Table 2, we observe that our method has superior visual quality compared to HiDDeN and 3D-DWT.

4.3. Robustness-Quality-Payload Trade-off

As mentioned in Section 1, a comprehensive evaluation of a watermarking system requires thorough analysis of the model's payload, robustness, as well as quality. In this section, we visualize this trade-off by fixing either payload or quality, and studying the relationship between the remaining two variables. We use the decoding accuracy as a measure of robustness, PSNR as a measure of quality, and message length for payload. Since the relations also depend on the type of distortion applied to the videos, we select four representative distortions from different categories, namely H.264 compression (CRF=22), spatial cropping (p=0.5), frame drop (p=0.5), and also Gaussian noise (std=0.06), and compute the average decoding accuracy as a measure of robustness.

Figure 7 and Figure 8 shows the trade-off between

	Identity	H.264 (CRF=22)	Frame Average (N=3)	Frame Drop (p=0.5)	Frame Swap (p=0.5)	Gaussian Blur (2.0)	Gaussian Noise (0.04)	Random Crop (0.4)	Random Hue (1.0)	Average
HiDDeN	99.10	79.85	96.91	**99.03**	99.10	72.70	91.27	95.27	98.98	92.47
3D-DWT	99.69	89.29	96.78	79.85	90.15	92.78	**99.01**	71.38	**99.59**	90.95
DVMark	**99.99**	**92.94**	**98.10**	98.99	**99.35**	**98.09**	98.56	**97.06**	**99.81**	**98.10**

Table 1: Comparison of Bit Accuracy for different watermarking methods. From top to down, we present the bit accuracy evaluated on 500 random videos for HiDDeN, 3D-DWT, and DVMark (our method), on a variety of common distortions.
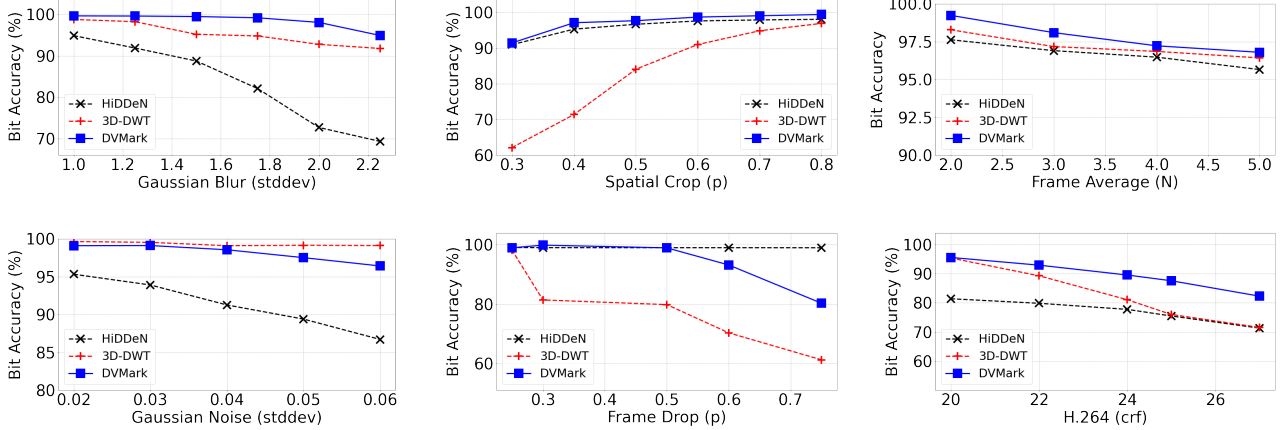

Figure 6: Bit accuracy for 3D-DWT, HiDDeN, and DVMark for various distortions and distortion strengths. For spatial crop, p is the ratio of the cropped box width over the original width, while keeping aspect ratio. For frame drop, p is the proportion of frames randomly dropped from the watermarked video.

	PSNR ↑	MSSIM ↑	LPIPS x 100 ↓	tLP x 100 ↓	MOS ↑
3D-DWT	36.5	0.983	8.79	0.628	0.90
HiDDeN	35.5	0.962	8.92	0.354	0.86
DVMark	**37.0**	**0.985**	**5.70**	**0.160**	**0.92**

Table 2: Quality metrics for videos watermarked by 3D-DWT, HiDDeN, and DVMark.

quality-robustness (for a fixed payload) and payload-robustness (for a fixed quality) respectively. We see that our method is superior to the both 3D-DWT and HiDDeN by a significant margin across both the robustness-quality as well as robustness-payload curves. For Figure 7, we fix the payload to be $m = 96$, and adjust the watermark strength α to vary the quality. For Figure 8, we train a separate model for each payload, and adjust the watermark strength so that the resulting average PSNR is around 37dB.
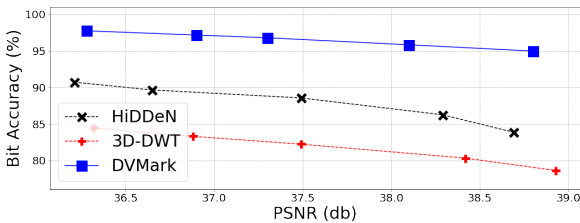

Figure 7: PSNR versus average bit accuracy for DVMark and other methods compared. The curves are generated by adjusting the watermark strength parameter α without re-training the model.
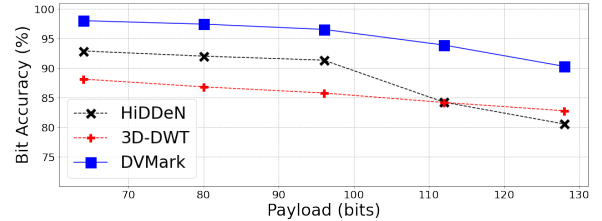

Figure 8: Payload versus average bit accuracy for DVMark and other methods compared.

4.4. Performance on Larger Videos

A practical watermarking solution must work for a variety of video resolutions and lengths. We demonstrate in this section that our method works out-of-the-box for larger and longer videos. We apply our models fully convolutionally on spatial dimensions, and apply the encoder every $T = 8$ frames. Namely, for a video sequence of size $T \times H \times W$, we divide the video to segments of $8 \times H \times W$, and apply DVMark to each of these segments with the same embedded message. We note that in theory our model is fully convolutional in the temporal dimension as well, but we empirically observe that the model performs better with applying to temporal segments. A possible explanation is due to the limited number of frames $T = 8$ at training time.

Same as in Section 4.3, we compute the average decoding accuracy over four distortions (H.264, crop, frame

Length (T) / Resolution ($H \times W$)	128×128	462×240	864×480
$T = 8$	96.14	96.63	95.29
$T = 16$	96.60	97.07	96.00
$T = 32$	96.80	97.16	96.01
$T = 64$	96.80	97.19	96.18

Table 3: Decoding accuracy for DVMark applied to various video resolutions and video lengths. Model accuracy is averaged across four types of distortions (H.264, crop, frame drop, Gaussian noise).

drop, Gaussian noise) for a matrix of different resolutions and video lengths. From the results in Table 3, we observe no performance degradation when our method is applied to larger videos in general.

4.5. Detector in a Video Editing Application

In this section, we evaluate the performance of the watermark detector. The watermark detector head is trained on a mixture of watermarked and unwatermarked video clips. We evaluate the accuracy of the watermark detector on various distortions where we watermark half of the videos at random by the DVMark encoder in our eval set.

Identity	H.264 (CRF=22)	Frame Average (N=3)	Frame Drop (p=0.5)	Frame Swap (p=0.5)
99.75	94.27	97.10	99.75	98.89

Gaussian Blur (2.0)	Gaussian Noise (0.04)	Random Crop (p=0.4)	Random Hue (1.0)	**Average**
99.50	97.76	98.76	99.10	98.32

Table 4: Accuracy of the watermark detector under various video distortions.

Table 4 shows the prediction accuracy of our trained detector. We observe that the detector is able to differentiate between watermarked and unwatermarked video sequences with high accuracy despite the fact that the watermarked videos have good perceptual quality.

Video Editing Application Next we demonstrate the utility of the watermark detector through a video-editing application. Many modern videos (such as commentary videos) include the use of other original video sources during its creation. In the case that these original video sources are watermarked, it is important to identify and decode the watermarked message even in the presence of unwatermarked content.

We mimic the video editing pipeline of a commentary video by adding less than 1 second (16 frames) of watermarked source content to an unwatermarked background video of size 462×240 and of much longer lengths (e.g., T=720 frames). To simulate editing operations to the watermarked content, we center crop the watermarked video to 128×128 and apply a random saturation change to simulate the intermediate editing done by video editors. We finally place the edited source to the lower left corner of the cover video as shown in Figure 1. For the most extreme case in

our evaluation, the watermarked content consists only 0.5% of the total number of pixels in the final video.
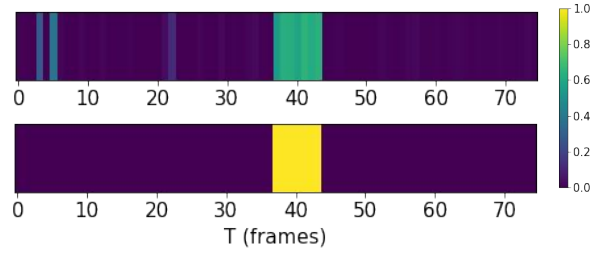

Figure 9: Visualization of the watermark detector predictions versus the ground truth. Top row: the probablity predicted by the watmermark detector. Bottom row: The ground truth labels for each frame, 1 indicates that a frame has been watermarked.

We apply the watermark detector to filter the background frames, where we remove frames with a confidence score less than 0.3 prior to passing the frames to the decoder. We see in Figure 9 that the detector is able to localize the watermarked video segment with great precision. This greatly improves the ability to decode the message compared to if we simply passed the full video sequence to the decoder, as shown in Table 5.

Background Length	T=60	T=120	T=240	T=360	T=720
With detector	99.62	98.81	98.50	95.32	90.02
Without detector	85.19	75.31	68.40	51.08	52.14

Table 5: The decoding accuracy of DVMark for the video editing application with and without detector pre-filtering, for different background video lengths. The background video is unwatermarked, and a watermarked video of length equal 16 frames is inserted to a random interval in the background video.

5. Conclusion

In this work, we propose DVMark, an end-to-end trainable framework for video watermarking. Our method consists of a novel multiscale design where the message is distributed across multiple spatial-temporal scales. Compared to both deep image watermarking and traditional watermarking methods, our method is more robust on a wide range of challenging video distortions, while maintaining good perceptual quality. Moreover, our method easily adapts to other distortion requirements through adding an additional distortion in our end-to-end framework. We further augment our framework with a watermark detector to locate watermarked video segments among unwatermarked content. Through rigorous evaluations, we demonstrate that our DVMark model serves as a practical and reliable solution for video watermarking.

References

[1] Loganathan Agilandeeswari and K Ganesan. A robust color video watermarking scheme based on hybrid embedding techniques. *Multimedia Tools and Applications*, 75(14):8745–8780, 2016. 2

[2] Mahdi Ahmadi, Alireza Norouzi, Nader Karimi, Shadrokh Samavi, and Ali Emami. Redmark: Framework for residual diffusion watermarking based on deep networks. *Expert Systems with Applications*, 146:113157, 2020. 2, 3

[3] Martin Arjovsky, Soumith Chintala, and Léon Bottou. Wasserstein gan. *arXiv preprint arXiv:1701.07875*, 2017. 3

[4] Md Asikuzzaman, Md Jahangir Alam, Andrew J Lambert, and Mark R Pickering. Robust DT CWT-based DIBR 3D video watermarking using chrominance embedding. *IEEE Transactions on Multimedia*, 18(9):1733–1748, 2016. 1, 2

[5] Md Asikuzzaman and Mark R Pickering. An overview of digital video watermarking. *IEEE Transactions on Circuits and Systems for Video Technology*, 28(9):2131–2153, 2017. 1, 2, 6

[6] Walter Bender, Daniel Gruhl, Norishige Morimoto, and Anthony Lu. Techniques for data hiding. *IBM Systems Journal*, 35(3&4):313–336, 1996. 2

[7] Patrizio Campisi and Alessandro Neri. Video watermarking in the 3d-dwt domain using perceptual masking. In *IEEE International Conference on Image Processing 2005*, volume 1, pages I–997. IEEE, 2005. 1, 2

[8] Joao Carreira, Eric Noland, Andras Banki-Horvath, Chloe Hillier, and Andrew Zisserman. A short note about kinetics-600, 2018. 5

[9] Joao Carreira and Andrew Zisserman. Quo vadis, action recognition? a new model and the kinetics dataset. In *proceedings of the IEEE Conference on Computer Vision and Pattern Recognition*, pages 6299–6308, 2017. 5

[10] Pik-Wah Chan and Michael R Lyu. A dwt-based digital video watermarking scheme with error correcting code. In *International Conference on Information and Communications Security*, pages 202–213. Springer, 2003. 2

[11] Deepshikha Chopra, Preeti Gupta, Gaur Sanjay, and Anil Gupta. Lsb based digital image watermarking for gray scale image. *IOSR Journal of Computer Engineering*, 6(1):36–41, 2012. 2

[12] Mengyu Chu, You Xie, Jonas Mayer, Laura Leal-Taixé, and Nils Thuerey. Learning temporal coherence via self-supervision for gan-based video generation. *ACM Transactions on Graphics (TOG)*, 39(4):75–1, 2020. 3, 6

[13] Lino E Coria, Mark R Pickering, Panos Nasiopoulos, and Rabab Kreidieh Ward. A video watermarking scheme based on the dual-tree complex wavelet transform. *IEEE Transactions on Information Forensics and Security*, 3(3):466–474, 2008. 2

[14] Ingemar J Cox, Joe Kilian, F Thomson Leighton, and Talal Shamoon. Secure spread spectrum watermarking for multimedia. *IEEE Transactions on Image Processing*, 6(12):1673–1687, 1997. 5

[15] Ingemar J Cox, Matthew L Miller, Jeffrey Adam Bloom, and Chris Honsinger. *Digital Watermarking*, volume 53. Springer, 2002. 2

[16] Frederic Deguillaume, Gabriela Csurka, Joseph JK O'Ruanaidh, and Thierry Pun. Robust 3d dft video watermarking. In *Security and Watermarking of Multimedia Contents*, volume 3657, pages 113–124. International Society for Optics and Photonics, 1999. 2

[17] Nilanjan Dey, Poulami Das, Anamitra Bardhan Roy, Achintya Das, and Sheli Sinha Chaudhuri. Dwt-dct-svd based intravascular ultrasound video watermarking. In *2012 World Congress on Information and Communication Technologies*, pages 224–229. IEEE, 2012. 2

[18] Ian Goodfellow, Jean Pouget-Abadie, Mehdi Mirza, Bing Xu, David Warde-Farley, Sherjil Ozair, Aaron Courville, and Yoshua Bengio. Generative adversarial nets. In *Advances in Neural Information Processing systems*, pages 2672–2680, 2014. 3

[19] Mohamed Hamidi, Mohamed El Haziti, Hocine Cherifi, and Driss Aboutajdine. A blind robust image watermarking approach exploiting the dft magnitude. In *IEEE/ACS 12th International Conference of Computer Systems and Applications*, pages 1–6. IEEE, 2015. 2

[20] Alain Hore and Djemel Ziou. Image quality metrics: Psnr vs. ssim. In *2010 20th International Conference on Pattern Recognition*, pages 2366–2369. IEEE, 2010. 6

[21] Mei Jiansheng, Li Sukang, and Tan Xiaomei. A digital watermarking algorithm based on DCT and DWT. In *The International Symposium on Web Information Systems and Applications*, page 104, 2009. 2

[22] Ton Kalker, Geert Depovere, Jaap Haitsma, and Maurice JJJB Maes. Video watermarking system for broadcast monitoring. In *Security and Watermarking of Multimedia contents*, volume 3657, pages 103–112. International Society for Optics and Photonics, 1999. 2

[23] S Katzenbeisser and FAP Petitcolas. *Digital Watermarking*. Springer, 2000. 2

[24] Will Kay, Joao Carreira, Karen Simonyan, Brian Zhang, Chloe Hillier, Sudheendra Vijayanarasimhan, Fabio Viola, Tim Green, Trevor Back, Paul Natsev, Mustafa Suleyman, and Andrew Zisserman. The kinetics human action video dataset, 2017. 5

[25] Hyung Shin Kim and Heung-Kyu Lee. Invariant image watermark using zernike moments. *IEEE transactions on Circuits and Systems for Video Technology*, 13(8):766–775, 2003. 2

[26] Somchok Kimpan, Attasit Lasakul, and Sakreya Chitwong. Variable block size based adaptive watermarking in spatial domain. In *IEEE International Symposium on Communications and Information Technology, 2004. ISCIT 2004.*, volume 1, pages 374–377. IEEE, 2004. 2

[27] Diederik P Kingma and Jimmy Ba. Adam: A method for stochastic optimization. *arXiv preprint arXiv:1412.6980*, 2014. 11

[28] Hongmei Liu, Nuo Chen, Jiwu Huang, Xialing Huang, and Yun Q Shi. A robust dwt-based video watermarking algorithm. In *2002 IEEE International Symposium on Circuits*

and Systems. Proceedings (Cat. No. 02CH37353), volume 3, pages III–III. IEEE, 2002. 2

[29] Yang Liu, Mengxi Guo, Jian Zhang, Yuesheng Zhu, and Xiaodong Xie. A novel two-stage separable deep learning framework for practical blind watermarking. In *Proceedings of the ACM International Conference on Multimedia*, pages 1509–1517. ACM, 2019. 3

[30] Mario Lucic, Karol Kurach, Marcin Michalski, Sylvain Gelly, and Olivier Bousquet. Are gans created equal? a large-scale study. In *Advances in Neural Information Processing Systems*, pages 700–709, 2018. 5

[31] Xiyang Luo, Ruohan Zhan, Huiwen Chang, Feng Yang, and Peyman Milanfar. Distortion agnostic deep watermarking. In *Proceedings of the IEEE Conference on Computer Vision and Pattern Recognition*, pages 13548–13557, 2020. 1, 3

[32] Majid Masoumi and Shervin Amiri. A blind scene-based watermarking for video copyright protection. *AEU-International Journal of Electronics and Communications*, 67(6):528–535, 2013. 2, 5

[33] Aayush Mishra, Suraj Kumar, Aditya Nigam, and Saiful Islam. Vstegnet: Video steganography network using spatio-temporal features and micro-bottleneck. In *The British Machine Vision Conference*, page 274, 2019. 3

[34] Takeru Miyato, Toshiki Kataoka, Masanori Koyama, and Yuichi Yoshida. Spectral normalization for generative adversarial networks. *International Conference on Learning Representations*, 2018. 3, 5

[35] Joseph JK O'Ruanaidh and Thierry Pun. Rotation, scale and translation invariant digital image watermarking. In *Proceedings of International Conference on Image Processing*, volume 1, pages 536–539. IEEE, 1997. 2

[36] Swati Patel, Anilkumar Katharotiya, and Mahesh Goyani. A survey on digital video watermarking. *International Journal Comp. Tech. Appl*, 2(6):3015–3018, 2011. 2

[37] Masaki Saito, Shunta Saito, Masanori Koyama, and Sosuke Kobayashi. Train sparsely, generate densely: Memory-efficient unsupervised training of high-resolution temporal gan. In *International Journal of Computer Vision*, 2018. 5

[38] Richard Shin and Dawn Song. Jpeg-resistant adversarial images. In *Conference on Neural Information Processing Systems 2017 Workshop on Machine Learning and Computer Security*, 2017. 14

[39] Prabhishek Singh and RS Chadha. A survey of digital watermarking techniques, applications and attacks. *International Journal of Engineering and Innovative Technology*, 2(9):165–175, 2013. 2

[40] Mitchell D Swanson, Bin Zhu, and Ahmed H Tewfik. Multiresolution scene-based video watermarking using perceptual models. *IEEE Journal on Selected Areas in Communications*, 16(4):540–550, 1998. 2

[41] Kiyoshi Tanaka, Yasuhiro Nakamura, and Kineo Matsui. Embedding secret information into a dithered multi-level image. pages 216–220. IEEE, 1990. 2

[42] Matthew Tancik, Ben Mildenhall, and Ren Ng. Stegastamp: Invisible hyperlinks in physical photographs. *arXiv preprint arXiv:1904.05343*, 2019. 1, 2, 3

[43] Sergey Tulyakov, Ming-Yu Liu, Xiaodong Yang, and Jan Kautz. Mocogan: Decomposing motion and content for video generation. In *Proceedings of the IEEE conference on computer vision and pattern recognition*, pages 1526–1535, 2018. 3, 5

[44] Xintao Wang, Ke Yu, Shixiang Wu, Jinjin Gu, Yihao Liu, Chao Dong, Yu Qiao, and Chen Change Loy. Esrgan: Enhanced super-resolution generative adversarial networks. In *Proceedings of the European Conference on Computer Vision (ECCV)*, pages 0–0, 2018. 3

[45] Bingyang Wen and Sergul Aydore. Romark: A robust watermarking system using adversarial training. *Machine Learning with Guarantees Workshop at NeurIPS 2019*, 2019. 2

[46] Eric Wengrowski and Kristin Dana. Light field messaging with deep photographic steganography. In *Proceedings of the IEEE Conference on Computer Vision and Pattern Recognition*, pages 1515–1524, 2019. 2, 3

[47] Thomas Wiegand, Gary J Sullivan, Gisle Bjontegaard, and Ajay Luthra. Overview of the h. 264/avc video coding standard. *IEEE Transactions on Circuits and Systems for Video Technology*, 13(7):560–576, 2003. 2, 5

[48] Jing Zhang, Anthony TS Ho, Gang Qiu, and Pina Marziliano. Robust video watermarking of h. 264/avc. *IEEE Transactions on Circuits and Systems II: Express Briefs*, 54(2):205–209, 2007. 2

[49] Richard Zhang, Phillip Isola, Alexei A Efros, Eli Shechtman, and Oliver Wang. The unreasonable effectiveness of deep features as a perceptual metric. In *Proceedings of the IEEE Conference on Computer Vision and Pattern Recognition*, pages 586–595, 2018. 6

[50] Jiren Zhu, Russell Kaplan, Justin Johnson, and Li Fei-Fei. Hidden: Hiding data with deep networks. In *Proceedings of the European Conference on Computer Vision (ECCV)*, pages 657–672, 2018. 1, 2, 5

6. Additional Design and Experiment Details

6.1. Training Details

Distortions Layer: We apply a total of 10 differentiable distortions during training. The exact distortions include: CompressionNet (crf=25), random frame drop ($p = 0.5$), random frame swap ($p = 0.5$), random spatial crop ($p = 0.5$), random saturation change, random hue change, 3D-Gaussian blur ($\sigma = 2.0$), Gaussian Noise (std = 0.05), Differentiable JPEG ($q = 50$), and random frame shift, which is a random cyclic permutation of the temporal order. Each distortion is selected with equal probability during training.

Encoder-Decoder: We train all models with a batch size of 6 and video size $8 \times 128 \times 128$, using the ADAM [27] optimizer with an initial learning rate of 1e-4, and use an exponential decay with decay rate 0.8 every 200k steps. We train for a total of 3M steps. For the loss weights, we set the message loss weight $c_1 = 0.5$, the GAN generator loss weight $c_2 = 4e-3$. For training the GAN discriminator, we use the same learning rate but run $N = 2$ steps of the discriminator per every generator step. The watermark strength is set to $\alpha = 1.0$ during training.

To avoid spatial and temporal boundary artifacts from encoded videos, we symmetrically pad all of the convolution operations instead of zero-padding. We observe that zero or constant padding results in frames near the temporal boundary (e.g., frame 0 or frame 7) to be visually different from frames in the center, making the model less temporally stable.

Detector: As described in Section 3.2 of the main text, we train a detector to detect whether a segment of video frames are watermarked or not. The detector head consists of 4 Conv2D operations on top of the feature map D_f followed by a global pooling operation. The logit tensor prior to global pooling can also be used to provide more spatial and temporal granularity. Same as the encoder and decoder, the detector is trained on clips of size $8 \times 128 \times 128$ using the ADAM [27] optimizer with an initial learning rate of 1e-4, and use an exponential decay with decay rate 0.8 every 200k steps. We train for a total of 1M steps.

6.2. User Study Details

For the user study, raters are given the watermarked and original video in a side-by-side fashion, where raters are asked to choose whether the pair is "identical", or "different". Raters are encouraged to find difference in terms of noise, temporal flickering, saturation and color changes, as well as other types of differences. Raters are allowed to view the clips as many times as needed. The rating scale is defined as follows: the pair is "identical" if the rater is unable to find any difference given repeated viewings, "different" if the rater was able to spot some difference between the unwatermarked and watermarked videos.

6.3. WeightNet Architecture

In Section 3.2 of the main text, we presented WeightNet, a network that takes the cover video as input and outputs a normalized weight matrix W. WeightNet consists of three 3D-Conv layers, with number of channels $32, 64, 128$ with stride 2. The output is then globally averaged along the spatial and temporal dimensions, followed by a fully connected layer with $m \times 2$ number of units, with $m = 96$. Finally a softmax operation is applied such that the output $W_{ij} \in \mathbb{R}^{m \times 2}$ is row normalized.

6.4. Video GAN Architecture

Our video GAN discriminator consists of four sub-networks named ResBlock_i, one for each input scale. Each of the sub-networks consists of four residual 3D convolution layers, passed through a global pooling operation on T, W, H, and finally passed to a fully connected layer with output channel equal to 1. The residual layer is defined as follows. Given an input tensor X, the residual layer is defined as $R^{(c,s,t)}(X) = \text{conv}_{3\times3\times3}^{(c,s,t)}(X) + \text{conv}_{1\times1\times1}^{(c,s,t)}(X)$, $\text{conv}^{(c,s,t)}$ denotes a 3D convolution with stride (s, s, t) and number of output channels c. The output channel, spatial and temporal stride of the residual layers for each ResBlock_i is given in Table. 6.

Block	Channels	Spatial Strides	Temporal Strides
ResBlock$_1$	(32, 64, 128, 256)	(2, 2, 2, 2)	(1, 1, 1, 1)
ResBlock$_2$	(32, 64, 128, 256)	(2, 2, 2, 2)	(2, 1, 1, 1)
ResBlock$_3$	(32, 64, 128, 256)	(2, 2, 2, 1)	(2, 2, 1, 1)
ResBlock$_4$	(32, 64, 128, 256)	(2, 2, 1, 1)	(2, 2, 2, 1)

Table 6: Architecture parameters of the video GAN discriminator.

6.5. CompressionNet Architecture

In Section 3.2 of the main text, we presented CompressionNet as a differentiable proxy for video compression distortions. CompressionNet consists of seven layers of 3D convolutions. Each convolution layer has a kernel size of 3, and the number of units for each layer is shown in Figure 10. A residual connection is added from the input to the last layer. We train CompressionNet to mimic the output
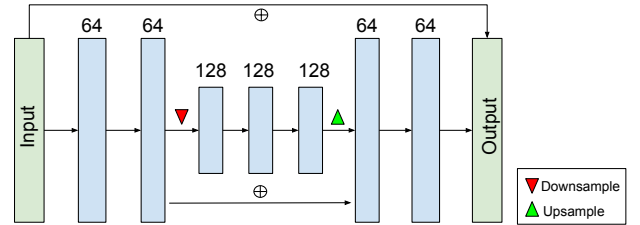

Figure 10: CompressionNet architecture. The numbers on top of each block are the output channels for each layer.

of an H.264 codec at a fixed Constant Rate Factor (CRF)

equal to 25. Same as in DVMark, we train CompressionNet on clips of size $8 \times 128 \times 128$.

7. Additional Detailed Results on Robustness, Quality, Payload

7.1. Robustness-Quality Tradeoff

PSNR	36.21	36.65	37.49	38.29	38.69
Acc. H.264 (CRF=22)	77.90	75.11	72.21	67.92	66.71
Acc. Crop (p=0.5)	95.48	95.16	94.14	92.92	89.31
Acc. Frame drop (p=0.5)	99.08	99.03	98.99	97.67	96.45
Acc. Gaussian noise (std=0.04)	90.37	89.29	88.89	86.50	83.03
Average	90.71	89.65	88.56	86.25	83.87

Table 7: Decoding accuracy of HiDDeN for four types of distortions for a range of PSNR values.

PSNR	36.28	36.90	37.33	38.12	38.81
Acc. H.264 (CRF=22)	93.74	92.98	92.54	89.49	87.02
Acc. Crop (p=0.5)	97.79	97.52	97.06	96.97	96.48
Acc. Frame drop (p=0.5)	99.17	99.15	98.98	98.96	98.91
Acc. Gaussian noise (std=0.04)	99.18	98.99	98.56	97.91	97.46
Average	97.74	97.16	96.79	95.83	94.97

Table 8: Decoding accuracy of 3D-DWT for four types of distortions for a range of PSNR values.

PSNR	36.32	36.88	37.49	38.42	38.93
Acc. H.264 (CRF=22)	86.48	82.91	79.46	73.17	68.06
Acc. Crop (p=0.5)	70.75	71.08	70.88	71.07	70.75
Acc. Frame drop (p=0.5)	81.02	79.71	79.15	77.84	76.89
Acc. Gaussian noise (std=0.04)	99.54	99.49	99.41	99.18	98.82
Average	84.45	83.30	82.23	80.32	78.63

Table 9: Decoding accuracy of DVMark for four types of distortions for a range of PSNR values.

In Tables 7 to 9, we provide the exact PSNR values and decoding accuracy values for four distortions (H.264, Crop, Frame drop, Gaussian noise) used to plot Figure 7 in the main text. While Figure 7 provides an overview of the robustness-quality trade-off of DVMark, HiDDeN, and 3D-DWT, we also provide these tables as a reference.

7.2. Robustness-Payload Tradeoff

In Tables 10 to 12, we provide the decoding accuracy values for four distortions (H.264, Crop, Frame drop, Gaussian noise), as well as the payload used to plot Figure 8 in the main text. While Figure 8 provides an overview of the robustness-payload trade-off of DVMark, HiDDeN, and 3D-DWT, we also provide these tables as a reference.

7.3. Performance on Larger Videos

In Tables 13 to 16, we present the performance of DV-Mark on various video lengths and resolutions on four dis-

Payload (bits)	64	80	96	112	128
Acc. H.264 (CRF=22)	80.44	79.61	79.85	69.23	60.97
Acc. Crop (p=0.5)	96.51	95.85	95.27	90.23	89.91
Acc. Frame drop (p=0.5)	99.54	99.36	99.03	93.10	91.21
Acc. Gaussian noise (std=0.04)	95.11	93.28	91.27	84.42	80.18
Average	92.9	92.03	91.35	84.25	80.56

Table 10: Decoding accuracy of HiDDeN for four types of distortions for a range of message lengths (payload).

Payload (bits)	64	80	96	112	128
Acc. H.264 (CRF=22)	93.01	92.90	92.94	89.03	84.63
Acc. Crop (p=0.5)	76.36	73.74	71.38	70.91	69.40
Acc. Frame drop (p=0.5)	83.29	81.20	79.85	77.69	78.03
Acc. Gaussian noise (std=0.04)	99.93	99.50	99.01	99.17	99.15
Average	88.15	86.84	85.80	84.2	82.80

Table 11: Decoding accuracy of 3D-DWT for four types of distortions for a range of message lengths (payload).

Payload (bits)	64	80	96	112	128
Acc. H.264 (CRF=22)	93.50	93.11	92.94	88.07	83.09
Acc. Crop (p=0.5)	98.72	98.10	97.06	94.21	87.72
Acc. Frame drop (p=0.5)	99.90	99.12	97.64	97.04	96.82
Acc. Gaussian noise (std=0.04)	99.95	99.43	98.56	96.28	93.57
Average	98.02	97.44	96.55	93.9	90.3

Table 12: Decoding accuracy of DVMark for four types of distortions for a range of message lengths (payload).

tortions (H.264, crop, frame drop, Gaussian noise). The average of these values are already shown in Table 3 in the main text.

Length (T) / Resolution ($H \times W$)	128×128	462×240	864×480
$T = 8$	92.94	92.25	86.15
$T = 16$	93.02	93.18	88.26
$T = 32$	92.98	93.20	88.32
$T = 64$	92.96	93.19	88.73

Table 13: Decoding accuracy for DVMark applied to various video resolutions and video lengths with H.264 distortion with CRF=22.

Length (T) / Resolution ($H \times W$)	128×128	462×240	864×480
$T = 8$	96.46	98.77	99.60
$T = 16$	97.35	98.82	99.54
$T = 32$	97.58	98.89	99.57
$T = 64$	97.52	98.90	99.55

Table 14: Decoding accuracy for DVMark applied to various video resolutions and video lengths with spatial crop with crop ratio 0.4.

We note that the effect of adjusting the video resolution (from the same source video) is a trade-off between more spatial redundancy versus less high-frequency regions in the image. In terms of distortions, the effects of increasing resolution are distortion dependent. For crop and frame drop, increasing spatial resolution in general improves the decoding accuracy, whereas for Gaussian noise, the effect is neu-

Length (T) / Resolution ($H \times W$)	128×128	462×240	864×480
$T = 8$	96.59	96.95	97.01
$T = 16$	97.51	97.64	97.75
$T = 32$	97.91	97.98	98.01
$T = 64$	98.02	98.09	98.02

Table 15: Decoding accuracy for DVMark applied to various video resolutions and video lengths with frame drop distortion (p=0.5).

Length (T) / Resolution ($H \times W$)	128×128	462×240	864×480
$T = 8$	98.56	98.53	98.38
$T = 16$	98.51	98.64	98.41
$T = 32$	98.72	98.60	98.44
$T = 64$	98.69	98.60	98.42

Table 16: Decoding accuracy for DVMark applied to various video resolutions and video lengths with Gaussian Noise with std-dev=0.04.
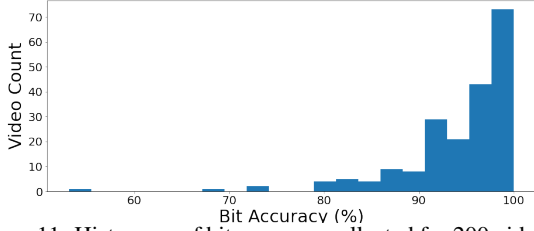

Figure 11: Histogram of bit accuracy collected for 200 video clips of length 8 and resolution 128×128. We apply the DVMark encoder and distort the video by applying Gaussian noise with a standard deviation of 0.06.

tral. For H.264, we see a slight drop for the largest video resolution. For video length, we see that a longer video increases the decoding accuracy for all video resolutions and distortion types.

8. Ablation Studies

8.1. A Study of Per-video Robustness

The content of a video is certainly an important factor for the performance of any watermarking method, but is rarely discussed in the literature. We study for which videos the model performs the best and worst in terms of the decoding accuracy.

Figure 11 plots the histogram of decoding accuracy aggregated over 200 videos clips with length equal 8 frames. To avoid accuracy values concentrating at 100.0%, we apply a the Gaussian Noise distortion with standard deviation 0.06 to make the decoding more challenging.

We note that while the majority of the clips have accuracy higher than 90%, there are a few examples with relatively low accuracy. We visualize these examples in Figure 12. We observe that videos with less high frequency components (e.g., blurry videos) and with less motion perform worse than videos with more texture and more motion.

Figure 12: Samples of video clips with low decoding accuracy versus high decoding accuracy. The bit accuracy of the example clip is given in the numbers below each frame.

This aligns well with the intuition that videos with "richer" content are easier to watermark.

8.2. Network Architecture

In this section, we demonstrate the effectiveness of our multi-head design. Table 17 shows the decoding accuracy of various design choices over various distortions. We observe that the multiscale components improve the robustness of the overall method.

Payload (bits)	Head1	Head2	Head1 + Head2	Head1 + Head2 +WeightNet
Identity	99.80	99.81	99.76	99.85
H.264 (crf=22)	88.26	87.74	92.85	92.94
Gaussian Noise (std=0.04)	94.57	96.00	96.79	97.07
Average	94.21	94.52	96.47	96.62

Table 17: Decoding accuracy of several variations of the network design. "Head1" and "Head2" refers to the case where one of the decoder heads is removed. "Head1 + Head2" refers to the case where we use both decoder heads but simply sum the output without weighting. "Identity" distortion refers to the case where no distortion is applied.

8.3. Loss Function Weights

In this section, we investigate how the various weights c_1 and c_2 in the loss function (Equation 5 in the main text) affect the trained model. The loss function is defined as

$$L_{total} = L_I(V_{in}, V_w) + c_1 L_M(M, M^w) + c_2 L_G(V_w), \quad (6)$$

with c_1 being the message loss weights and c_2 being the GAN loss.

c_1 controls the trade-off between quality and robustness. Table 18 shows the decoding accuracy and PSNR of the model when c_1 is varied. We fix the other hyper-parameters same as in Section 1.1.

c_2 controls the scale of the perceptual quality versus L_2 loss. Figure 13 shows that lower GAN weight tends to generate noisier watermarks that are less aesthetically pleasing.

Message Loss Weight	$c_1 = 0.1$	$c_1 = 0.3$	$c_1 = 0.5$	$c_1 = 0.7$
Accuracy	85.3	92.2	96.6	98.7
PSNR	39.1	37.8	36.8	34.2

Table 18: Decoding accuracy versus PSNR for various message loss weight c_1. The accuracy is computed as an average of Identity, H.264, and Gaussian Noise distortions.
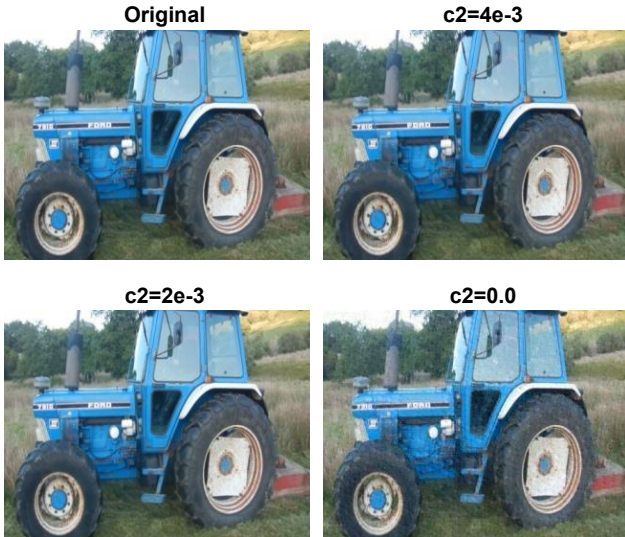

Figure 13: Samples of the original frame and watermarked frames with varying GAN loss weight c_2. Note that frames without the GAN loss ($c_2 = 0.0$) are much noisier visually.

8.4. CompressionNet

To evaluate the effectiveness of various approaches for improving robustness to video compression, we compare the performance of CompressionNet with several other alternative methods that dampen the high-frequency components of a video. The methods selected are 3D and 2D Gaussian blurring, frequency truncation, and differentiable JPEG [38]. For 2D and 3D Gaussian blur, we use a Gaussian kernel with spatial kernel size 5 and standard deviation 2.0. We use a temporal kernel size 3 for 3D Gaussian blur. For differentiable JPEG, we set a quality factor of $q = 50$ with chroma-subsampling enabled. For frequency truncation, we apply a 3D-FFT and set the coefficient outside a cube of width $0.5T \times 0.5H \times 0.5W$ to 0. Table 19 shows that while these methods are effective to some extent at providing robustness against compression, they are less effective compared to CompressionNet.

	3D-Blur	2D-Blur	Diff-JPEG	Identity	Compression-Net	Combined
CRF=22	78.1	75.6	72.4	53.5	89.3	93.0

Table 19: Bit accuracy on H.264 video compression for models trained with different types of differentiable distortions.

9. Visual Examples

More visual samples from DVMark, as well as HiDDeN and 3D-DWT can be found in fsup 14 to 19. Note that the "Difference" image (third row) is the *scaled* difference (normalized to 0-1) between the watermarked and cover frames. Thus the magnitude does not reflect the absolute value of the difference. The difference map serves only as a visualization of where the information is embedded in the signal.
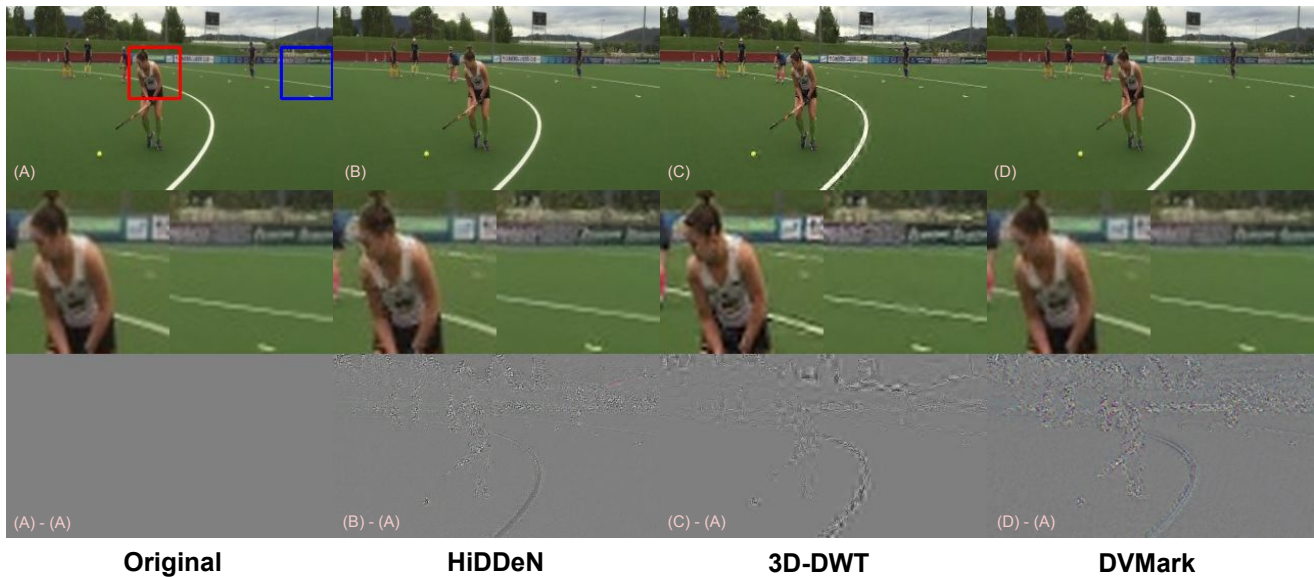
| Original | HiDDeN | 3D-DWT | DVMark |

Figure 14: Visual samples 1 of original and watermarked video frames from various watermarking methods. The second row contains a zoomed in view to better display the details. Note the "Difference" image (third row) is the *scaled* to 0-1 for each example, and thus the magnitude does not reflect the absolute value of the difference.
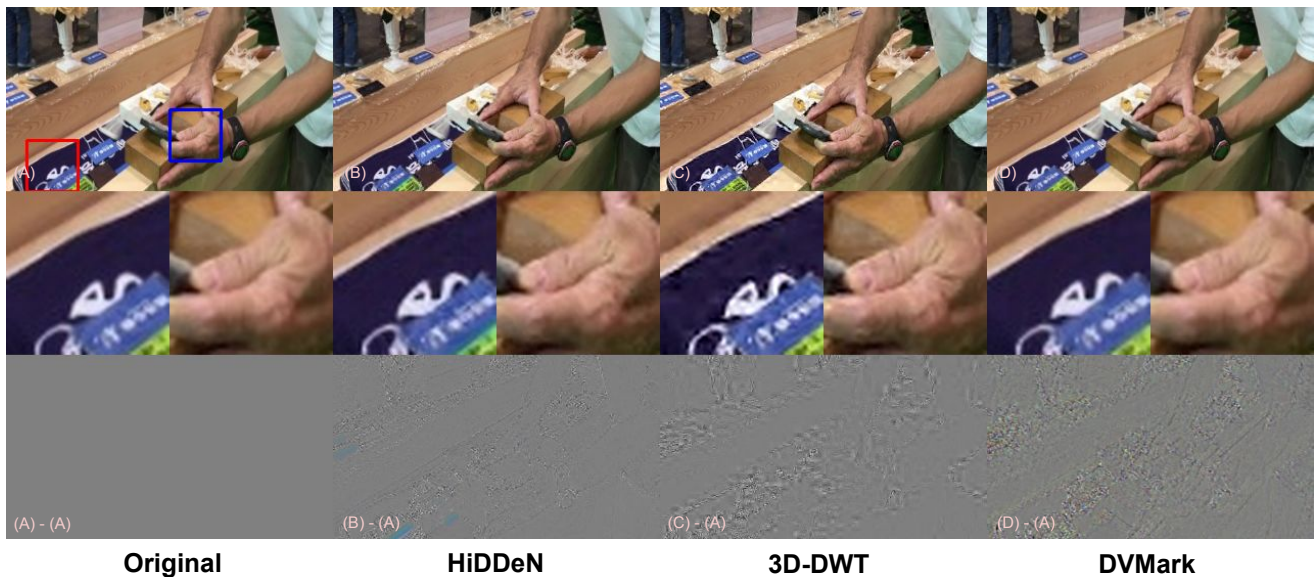

| Original | HiDDeN | 3D-DWT | DVMark |

Figure 15: Visual samples 2 of original and watermarked video frames from various watermarking methods. The second row contains a zoomed in view to better display the details. Note the "Difference" image (third row) is the *scaled* to 0-1 for each example, and thus the magnitude does not reflect the absolute value of the difference.

| Original | HiDDeN | 3D-DWT | DVMark |

Figure 16: Visual samples 3 of original and watermarked video frames from various watermarking methods. The second row contains a zoomed in view to better display the details. Note the "Difference" image (third row) is the *scaled* to 0-1 for each example, and thus the magnitude does not reflect the absolute value of the difference.
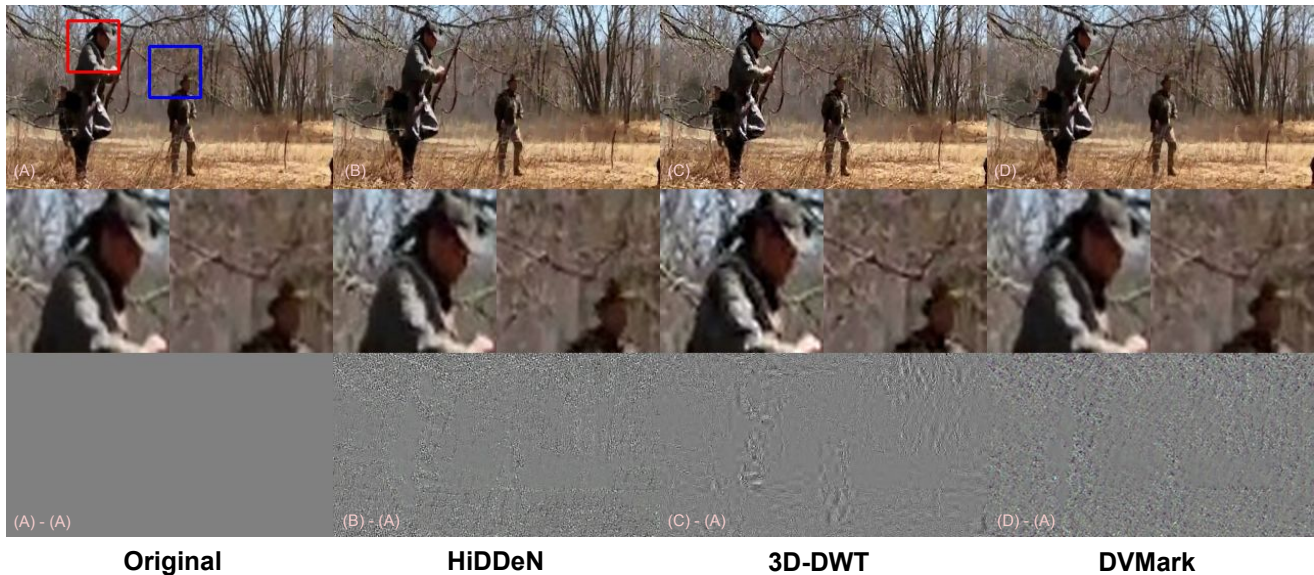

| Original | HiDDeN | 3D-DWT | DVMark |

Figure 17: Visual samples 4 of original and watermarked video frames from various watermarking methods. The second row contains a zoomed in view to better display the details. Note the "Difference" image (third row) is the *scaled* to 0-1 for each example, and thus the magnitude does not reflect the absolute value of the difference.
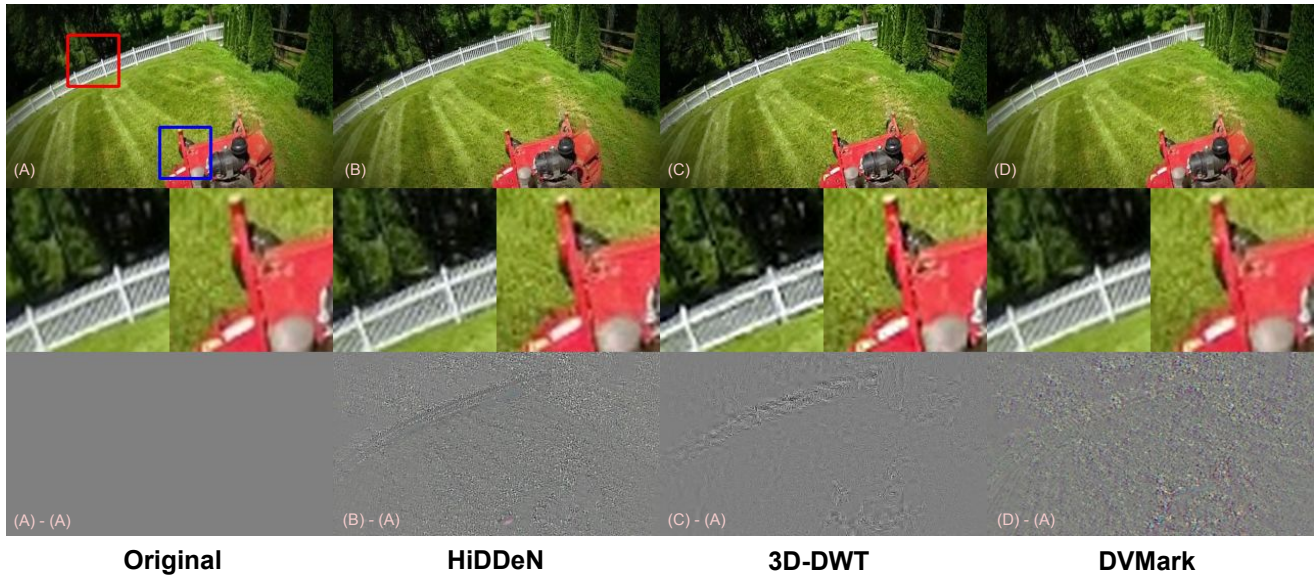
Original **HiDDeN** **3D-DWT** **DVMark**

Figure 18: Visual samples 5 of original and watermarked video frames from various watermarking methods. The second row contains a zoomed in view to better display the details. Note the "Difference" image (third row) is the *scaled* to 0-1 for each example, and thus the magnitude does not reflect the absolute value of the difference.
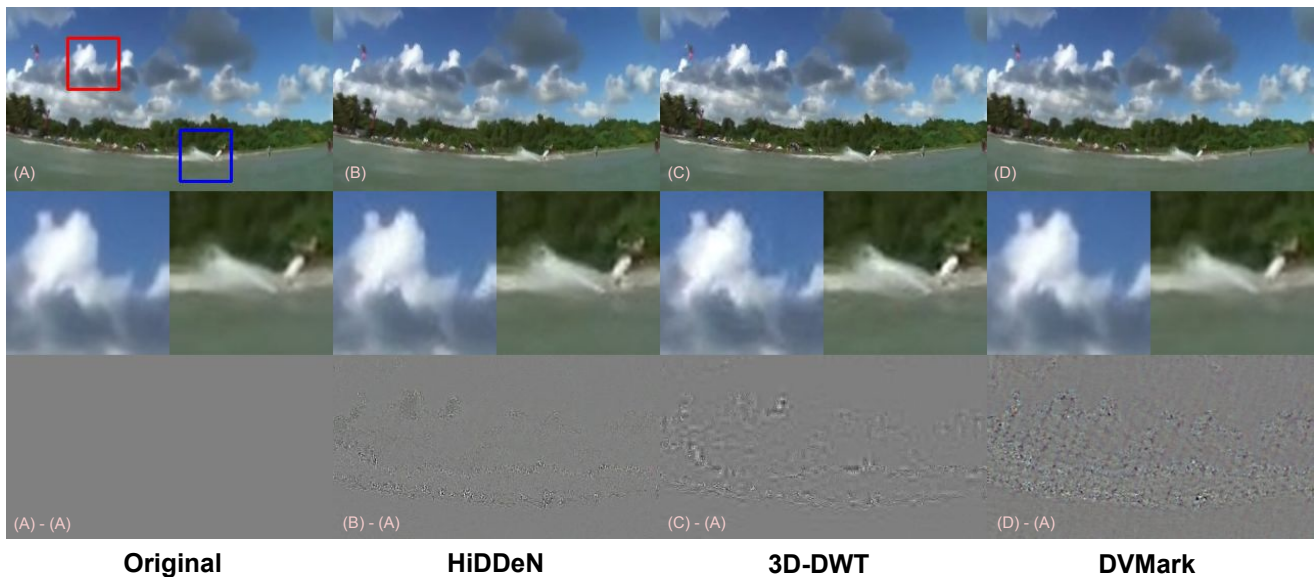

Original **HiDDeN** **3D-DWT** **DVMark**

Figure 19: Visual samples 6 of original and watermarked video frames from various watermarking methods. The second row contains a zoomed in view to better display the details. Note the "Difference" image (third row) is the *scaled* to 0-1 for each example, and thus the magnitude does not reflect the absolute value of the difference.